Metabolism and carbonate buffering drive seasonal dynamics of CO_2 emissions from two German reservoirs

Peifang Leng [1 2], Matthias Koschorreck [2]

1 Key Laboratory of Ecosystem Network Observation and Modeling, Institute of Geographic Sciences and Natural Resources Research, Chinese Academy of Sciences, Beijing, 100101, China

2 Department of Lake Research, Helmholtz Centre for Environmental Research-UFZ, Brückstr. 3a, 39114 Magdeburg, Germany

Corresponding author: Peifang Leng, peifang.leng@ufz.de, Brückstr. 3a, 39114 Magdeburg, Germany

Abstract

Biological metabolism drives much of the variation in CO_2 in terrestrial ecosystems but does not explain CO_2 oversaturation and emission in net autotrophic lakes and reservoirs. The unexplained CO_2 could be attributed to the equilibria between CO_2 and the carbonate buffering system, which is seldom integrated into CO_2 budgets, let alone its interplay with metabolism on CO_2 emissions. Here, we perform a process-based mass balance modeling analysis based on an 8-year dataset from two adjacent reservoirs with similar catchment sizes but contrasting trophic states and alkalinity. We find that in addition to the well-acknowledged driver of net metabolic CO_2 production, carbonate buffering also determines the total amount and seasonal dynamics of CO_2 emissions from the reservoirs. Carbonate buffering can contribute up to nearly 50% of whole-reservoir CO_2 emissions, by converting the ionic forms of carbonate to CO_2. This results in similar seasonal CO_2 emissions from reservoirs with differing trophic state, even in low alkalinity system. We therefore suggest that catchment alkalinity, instead of trophic state, may be more relevant in predicting CO_2 emissions from reservoirs. Our model approach highlights the important role of carbonate buffering and metabolism that generate and remove CO_2 throughout the reservoirs on a seasonal scale. The inclusion of carbonate buffering could diminish a major uncertainty in the estimation of reservoir CO_2 emissions and increase the robustness of aquatic CO_2 emission estimates.

Introduction

Carbon dioxide (CO_2) is the dominant gaseous end product of the C cycling and the largest contributor to the anthropogenic greenhouse effect (IPCC, 2022). Damming of lotic water, which is essential for human welfares, deeply affects the freshwater carbon footprint by facilitating internal processing with longer water residence time. Reservoirs are typically supersaturated in CO_2 relative to atmosphere (Deemer et al., 2016; Stets et al., 2009), making them a CO_2 source, while some studies suggest that eutrophic reservoirs and lakes can turn into CO_2 sinks due to increases in aquatic primary productivity (Bogard and Del Giorgio, 2016; Jones et al., 2016). Reservoirs are responsible for substantial increases of the global lake area (Pi et al., 2022), highlighting the critical need for precise quantification of CO_2 emissions from reservoirs. Currently, net ecosystem production (NEP) is usually considered as the main driver of CO_2 supersaturation in reservoirs, thus trophic states, as the indicator of NEP, is widely applied as a robust proxy to estimate global lake and reservoir CO_2 emissions (DelSontro et al., 2018; Kortelainen et al., 2006; Trolle et al., 2012). However, recent observations of CO_2 dynamics in rivers and lakes indicate that net autotrophic systems also emit CO_2 (Bogard and Del Giorgio, 2016; McDonald et al., 2013; Stets et al., 2017), suggesting that metabolism alone is not sufficient in explaining CO_2 emissions in lakes and reservoirs (Marcé et al., 2015; Weyhenmeyer et al., 2015). The underlying processes that sustain CO_2 emissions from the productive reservoirs are, however, still far from being understood.

Whether a given system emits or consumes CO_2 depends on the net balance of external inputs/outputs and in-reservoir production/consumption via biological and chemical processes. All carbon entering reservoirs can be converted to CO_2 via three distinct pathways (**Fig. 1**a): 1) direct CO_2 input from external inflows (inflows, lateral soils, and groundwater), 2) biotically via net metabolic CO_2 production within reservoir, and 3) abiotically via carbonate buffering (Duvert et al., 2019; Stets et al., 2017). Direct external CO_2 can be derived from terrestrial organic carbon (OC) mineralization and catchment weathering, fueling intense aquatic CO_2 emission to the atmosphere (Duvert et al., 2019; Weyhenmeyer et al., 2015; Xiao et al., 2020). Net metabolic CO_2 production is the sum of all biotic processes that convert other forms of carbon (particulate organic carbon, POC; dissolved organic carbon, DOC; particulate inorganic carbon, PIC) to dissolved inorganic carbon (DIC), including whole-reservoir respiration, photosynthesis, anaerobic respiration, and photochemical DOC mineralization. In reservoirs with high DOC concentrations where external DOC input is the major contributor, higher net heterotrophy (respiration exceeding photosynthesis) is usually observed (Allesson et al., 2021; Bogard and Del Giorgio, 2016; Lapierre et al., 2013). In contrast, increased terrestrial nutrient delivery is known to stimulate in-

lake productivity by enhancing growth of phototrophs, leading to higher CO_2 consumption (Li et al., 2021).

Although seasonal patterns in net metabolic CO_2 production have been widely observed (Trolle et al., 2012; Vachon et al., 2017), the external derived CO_2 from carbonate buffering in supporting reservoir emissions, however, is seldom distinguished, especially regarding their variations in time (Vachon and Del Giorgio, 2014). External inorganic carbon inputs vary seasonally due to dynamic hydrologic regimes and soil respiration in the catchments (Chaplot and Mutema, 2021; Tittel et al., 2015). Meanwhile, the carbonate equilibrium also strongly modulates CO_2 in reservoirs based on the speciation of DIC (Marcé et al., 2015). In freshwaters with high pH/alkalinity, CO_2 is in equilibrium with the ionized forms, HCO_3^- and CO_3^{2-} (Stets et al., 2017), decoupling CO_2 dynamics from internal metabolism. Carbonate buffering (by converting dissolved CO_2 into ionic forms, and vice versa), therefore, may contribute a large fraction of CO_2 evading to the atmosphere via large inorganic carbon import from catchments.

Given the seasonality of nutrient loads from catchments (Leng et al., 2021; Tittel et al., 2015), we assume lower metabolic CO_2 production (net autotrophy) and higher external DIC inputs partially offset each other, resulting in more stable CO_2 emissions from eutrophic reservoirs (**Fig. 1**b). Primary production, enhanced by increases in phytoplankton productivity, depletes CO_2 and enhances pH in nutrient-rich reservoirs during summer (Li et al., 2021). When external DIC loading from catchments contributes to the system, DIC input or removal will change carbonate equilibrium and CO_2 fluxes. However, little is known about the extent to which carbonate buffering contributes to CO_2 evasion on a seasonal scale. Particularly, when alkalinity is low (0-1 meq L^{-1}), metabolic CO_2 production has been thought to be the major driver of CO_2 dynamics (Khan et al., 2020). It is still unclear whether carbonate buffering has the potential to reverse CO_2 undersaturation to supersaturation, bringing large uncertainty in CO_2 emission estimates.

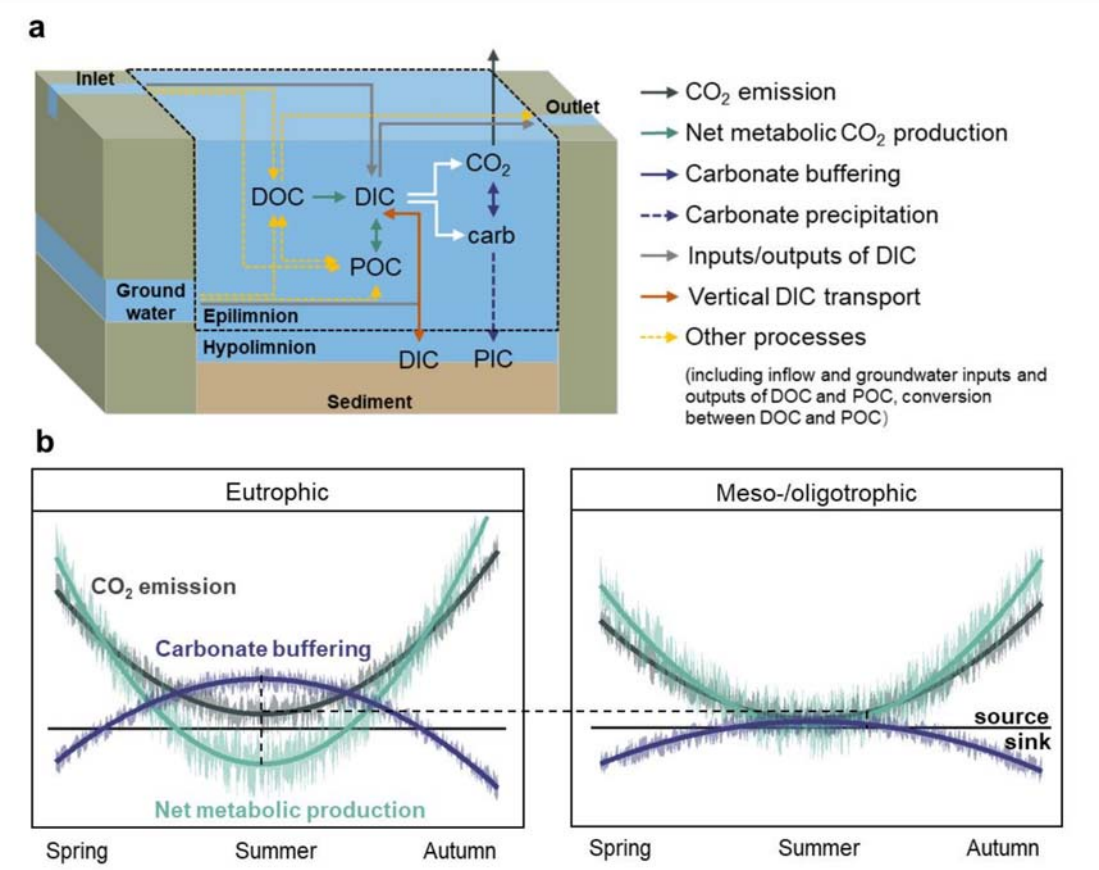

Figure 1. Model diagram and hypotheses. **a.** Scheme of C sources, forms, and biogeochemical transformations in epilimnion for the stratified reservoir systems or entire water column for the unstratified systems. The dashed black line represents the model boundary. The white arrows represent that dissolved organic carbon (DIC) consisting of carbonates (indicated by "carb", HCO_3^- + CO_3^{2-}) and CO_2. DOC, dissolved organic carbon; POC, particulate organic carbon; PIC, particulate inorganic carbon. **b.** Hypothetical responses of CO_2 emissions to seasonal-dependent processes in reservoirs with contrasting productivity and alkalinity. The seasonal change in CO_2 emissions is governed by the balance of in-reservoir processes and external inputs: net metabolic CO_2 production (green lines) and carbonate buffering (purple lines). Both processes can produce and consume CO_2 biotically and abiotically, respectively. The dashed black lines show different amounts of net metabolic CO_2 production and carbonate buffering from reservoirs with distinct trophic states result in the same CO_2 emissions.

Net metabolic CO_2 production and carbonate buffering are typically studied by comparison between rate of changes in O_2 and DIC (Khan et al., 2020; Marcé et al., 2015; Stets et al., 2017). This method interprets that the deviations of the theoretical slope (-1) between DO and DIC disequilibrium are caused by carbonate precipitation, therefore it largely overlooks: (1) the varying

respiratory/photosynthetic quotient (Trentman et al., 2023); (2) the effects of anerobic and photochemical processes, that potentially alter the correlation between DIC and O_2; and (3) low-alkalinity systems with seasonal fluctuation in the case of DIC inputs/removals. Biological net metabolic CO_2 production rates in reservoir are often assessed using diel measurements of free-water dissolved O_2 capturing metabolic dynamics (Winslow et al., 2016). To evaluate the role of all processes which may govern CO_2 dynamics in the reservoir ecosystems, we established a coupled DIC and CO_2 mass balance using in-situ measures of DIC and CO_2 at a temporal resolution that captures seasonal variation. The estimates of net metabolic CO_2 production can be achieved by the balance between CO_2 emissions and the difference between DIC inputs and outputs. By contrasting the DIC mass balance with the CO_2 one, we are able to quantify the effect of carbonate buffering on reservoir estimates of CO_2 processing.

The aim of this study is to disentangle the seasonal patterns of CO_2 dynamics and to quantify the relative contribution of the key underlying biotic and abiotic processes that drive seasonal pattern in CO_2 emissions. To reconstruct the seasonal dynamics of these processes supporting CO_2 emission, we selected two adjacent temperate reservoirs with contrasting trophic states (eutrophic and mesotrophic) and collected samples at biweekly interval for more than 8 years. We hypothesized (1) a seasonal succession in the relative contributions of each process influencing reservoir CO_2 budgets (only epilimnion during stratification), and (2) eutrophication accompanied by external inorganic carbon loading resulting in attenuated seasonal variation in CO_2 emissions. We built a simple mass balance model coupling reservoir DIC and CO_2 budgets using the routine monitoring data to realistically interpolate rates of different pathways supporting CO_2 evasions. In addition, we validated our mass balance approach by comparing the net metabolic CO_2 production with the NEP estimated from free-water oxygen measurements. Finally, we developed a statistical model to explore how sensitive reservoir CO_2 dynamics may be to climatic drivers (flow discharge and sunlight duration of the day) and major biotic and abiotic processes.

Methods

Stream-reservoir systems

The Hassel and Rappbode catchments are located in the eastern Harz Mountains in Central Germany. Both catchments share similar catchment size and morphological properties (40.5 and 39.1 km^2 for Hassel and Rappbode, respectively). The Hassel catchment is more affected by agriculture (37% forest and 25% agricultural fields) while Rappbode is primarily forested (72% forest and 2% agricultural fields, **Fig. S1**) (Friese et al., 2014). This explains the distinct trophic states in Hassel (eutrophic, **Fig. S1**) and Rappbode (mesotrophic)

reservoirs (Kong et al., 2022). The inflow streams Hassel and Rappbode drain directly into the pre-dam reservoirs Hassel and Rappbode, respectively (referred to as "Hassel Reservoir" and "Rappbode Reservoir" hereafter). The reservoirs were built to reduce sediment and nutrient load to the main reservoir of Rappbode, which is the largest drinking water reservoir in Germany. The Hassel and Rappbode reservoirs were brought into operation in 1960 and 1961, respectively (Wouters, 2011). Both reservoirs are configured with surface-release dams, resulting in constant water depth (**Fig. S1**). Thus, we assumed the same concentrations of solutes in surface reservoir water and outflow. Monitoring stations were located at the inflow streams and the reservoir surface close to the dam. As the water level in reservoirs in the dataset varied within 0.3 m in the studied years, we reasonably assumed that the surface area of reservoirs remained constant (0.26 km^2 in Hassel; 0.243 km^2 in Rappbode, Halbedel and Koschorreck (2013)).

Data collection

Biweekly measurements of water temperature, pH, alkalinity, total inorganic carbon (TIC), DOC, and total phosphorus (TP) were carried out from stream and reservoir monitoring sites for physical and chemical analysis in the field and laboratory from 2014 to 2021 (including ice-covered period). The lab methods and data handlings were described by Friese et al. (2014) in more detail.

Discharge data of both inflow streams were logged with 15-min intervals at the official automatic gauging station. At Hassel stream, the gauge is located 2 km upstream of the sampling site (51°41'54.0"N, 10°50'24.6"E). We corrected discharge assuming equal precipitation within the whole catchment (Wendt-Potthoff et al., 2014). The daily discharge of outflows of the pre-dam reservoirs was provided by the local dam operation company (Talsperrenbetrieb Sachsen-Anhalt, TSB). Meteorological data, including air pressure (hPa), air temperature (℃), precipitation (mm), wind speed (m s^{-1}), and solar radiation (J cm^{-2}) were collected at hourly interval from a weather station at Rappbode dam for both pre-dam reservoirs (weather station at YRA, see Friese et al. (2014)). Meteorological and discharge data were aggregated to daily mean values to match with other monitoring data for further analysis. The water residence time is defined as the ratio between the water volume of the reservoir and the daily inflow.

For CO_2 concentration, 30 mL of water samples were equilibrated with 30 mL N_2 or surrounding atmosphere in a gas tight syringe through vigorous shaking. N_2 was used as headspace gas before 2020 and the equilibrated gas was injected directly into the gas chromatograph (GC, SRI 8610, SRI Instruments, Torrance, USA). Since then, ambient air was used as headspace gas and the equilibrated gas was stored in evacuated Exetainer vails (Labco, UK) for later GC analysis

equipped with an auto sampler. Our previous work showed that both N_2 and ambient atmosphere as headspace gas generated identical CO_2 concentrations (Koschorreck et al., 2021). Ambient CO_2 concentrations and alkalinity were separately measured to correct the headspace CO_2 results due to the chemical equilibration of the carbonate system in syringes. The method can be implemented by using an R script provided by Koschorreck et al. (2021). Detailed methods for CO_2 analysis and calculation can be found in Leng et al. (2021). DIC was calculated from measured alkalinity, temperature, and pCO_2 by using the R package *seacarb* (Gattuso et al., 2021) using salinity constants of zero given the electrical conductivity < 400 µS cm^{-1} (at 25 °C) in all observations.

To model the dynamics of net ecosystem production (NEP), high temporal resolution measurements of physiochemical parameters were collected. We deployed an in-situ Zebra D-OPTO sonde (YSI6800, YSI, USA) suspended at 0.5m depth below the water's surface to measure water temperature and dissolved oxygen (O_2) at 15-min intervals. The O_2 logger was deployed from October 2015 to May 2016, July 2017 to December 2018, and March to December 2021. The O_2 logger was calibrated using 100% saturated O_2 water before and after deployment. Data were drift-corrected assuming a constant drift of the calibration during deployment. O_2 and CO_2 departure from atmospheric equilibrium (ΔO_2 and ΔCO_2) was calculated as the difference of O_2 and CO_2 concentrations in water and atmosphere.

Determination of CO_2 emissions

Flux rates (mmol CO_2 m^{-2} d^{-1}) were determined as the product of gas transfer velocities (k_{CO2}, m d^{-1}) and CO_2 concentration gradients (µmol L^{-1}) between water and air. The equations for k_{CO2} calculation in reservoirs are provided in *Supporting information* **Table S1**. *k* was estimated by the relationship between k_{600} and daily wind speed according to Crusius and Wanninkhof (2003). The k_{600} was then converted to a gas- and temperature-specific gas transfer velocity k_{CO2} using the temperature dependent Schmidt numbers for CO_2 (Crusius and Wanninkhof, 2003). We estimated the annual CO_2 flux (Mg C y^{-1}) for the pre-dam reservoirs Hassel and Rappbode by multiplying the mean surface area of the reservoirs by monthly averaged CO_2 fluxes.

Coupled CO_2-DIC modeling

We developed a simple process-based mass balance model based on the conservation of mass of CO_2 to estimate net metabolic CO_2 production and carbonate buffering capacity within the stream-reservoir system (**Fig. 1**a). The model boundary represents a completely mixed epilimnion (for stratified reservoirs) or unstratified reservoir. Changes of CO_2 between outlet and inlet are

theoretically caused by groundwater exchange, net metabolic CO_2 production (NMP, positive: production; negative: consumption), carbonate buffering (CB, positive: conversion of carbonates into CO_2; negative: conversion of CO_2 into carbonates), vertical CO_2 input (positive: vertical diffusion from deeper layers, including the input from hypolimnion to epilimnion during stratification and from sediment to mixed water column during mixing), and CO_2 emissions. The DIC mass balance can be calculated by accounting for changes in DIC pools resulting from groundwater exchange, NMP, vertical DIC input, and CO_2 emissions within reservoir. The biweekly mass balance model was run and the daily rates of different processes were smoothed by fitting multiple regressions in local neighborhood (loess). Process rates were presented as absolute daily rates (mmol $m^{-2}\,d^{-1}$) for parallel comparison by dividing the surface area of reservoirs. The mass balance model allows us to differentiate the carbonate buffering from potential in-reservoir metabolic production of CO_2, and therefore their relative contributions to CO_2 emissions. We parameterized the model using our own measurements and compiled all equations to solve for processes in CO_2 and DIC mass balance (**Table 1**). The detailed model parametrization processes are provided in *Supporting information* **Text S1**.

Table 1. Processes rates (mol d^{-1}) expressed in equations in the CO_2 and DIC mass balance model, where Q_{in} and Q_{out} are the discharge at the inlet and outlet, respectively. $[CO_{2in}]$ and $[CO_{2out}]$ are the CO_2 concentrations at the inlet and outlet, respectively. $[DIC_{in}]$ and $[DIC_{out}]$ are the DIC concentrations at the inlet and outlet, respectively. MLD represents the mixing layer depth. ΔVol is the volume of water transferred between hypolimnion and epilimnion. $[DIC_{hypo}]$ and $[DIC_{epi}]$ are the DIC concentrations at the hypolimnion and epilimnion, respectively. F_{CO2} is the CO_2 flux between air-water interface. A is the surface area of the reservoir. The detailed model parametrization are described in *Supporting information* **Text S1**.

Parameters	**Symbol**	**Equation**
Inflow CO_2 and DIC loads	$CO_{2,\,in}$ and DIC_{in}	$[CO_{2in}] \times Q_{in}$ and $[DIC_{in}] \times Q_{in}$
Outflow CO_2 and DIC loads	$CO_{2,\,out}$ and DIC_{out}	$[CO_{2out}] \times Q_{out}$ and $[DIC_{out}] \times Q_{out}$
Vertical input of DIC	DIC_v	MLD increase: $\Delta Vol \times [DIC_{hypo}]$ MLD increase: $\Delta Vol \times [DIC_{epi}]$
CO_2 emission	E	$F_{CO2} \times A$
Net metabolic CO_2 production	NMP	$[DIC_{out}] \times Q_{out} - C_{DIC,\,in} \times Q_{in} + F_{CO2} \times A$
Carbonate buffering	CB	$([DIC_{in}] - [CO_{2in}]) \times Q_{in} - ([DIC_{out}] - [CO_{2out}]) \times Q_{out}$

We made several simplifying assumptions in constructing the model. Vertical input can add or remove considerable DIC (and CO_2) to the DIC budgets,

especially during autumn turnover (Vachon et al., 2017). The diffusive exchange of solutes between epilimnion and hypolimnion in both studied reservoirs, however, is typically orders of magnitude slower than processes in the epilimnion (Kreling et al., 2014) and the vertical entrainment of DIC and CO_2 (DIC_v and $CO_{2,v}$) should be negligible compared to other biological and hydrological processes. We quantified more thoroughly this assumption by evaluating DIC mass transport (water column mixing) between layers when mixing layer changed (see *Results* and *Supporting information* Text S2 for further details). It should be noted that neglecting DIC_v would only affect estimates of net metabolic CO_2 production in our model, not carbonate buffering. We further calculate the potential role of vertical input on the mass balance model by comparing estimated NMP changes with and without the effect of vertical input.

We assumed that the contributions of CO_2 and DIC from groundwater can be neglected in our systems because the local geological units are covered with thin alluvium layers that are too thin to develop proper aquifers (Barth et al., 2017). The role of methane was excluded because its concentration and fluxes were generally three orders of magnitude lower than CO_2 (Tittel et al., 2019). To verify whether DIC converted to PIC (calcite precipitation) during carbonate buffering within the system, we estimated calcite saturation indices (SI) with measured concentrations of Ca^{2+} and HCO_3^- by using PHREEQC (Parkhurst and Appelo, 2013). For samples with higher SI (SI > 0), thermodynamics will favor calcite precipitation with 2 mol of carbonates producing 1 mol each of $CaCO_3$ ad CO_2. SI within the system ranged from -2.32 to -0.77 with the mean value of -1.56, implying calcite precipitation was not likely to occur in our reservoirs.

Ecosystem metabolism

We compared the NMP from mass-balance modeling with net ecosystem production (NEP) calculated from diel O_2 data using the LakeMetabolizer R package (Winslow et al., 2016). Reservoir NEP is the balance of gross primary production (GPP) and ecosystem respiration (ER), both of which influence diel oxygen concentration. We used the Bayesian model from Holtgrieve et al. (2010) considering hourly time series of dissolved oxygen, water temperature, wind speed, mixing layer depth (MLD), and photosynthesis active radiation (PAR). The MLD was calculated based on modeled water temperature profiles at daily time step throughout the study period in these two studied reservoirs (Kong et al., 2022), using the R package *RLakeAnalyzer* (Winslow et al., 2019). Missing values of mixing layer depth were checked for unstratified occurrences, then we used the depth of the reservoirs as the mixing layer depth instead. PAR (μmol m^{-2} s^{-1}) was calculated from solar radiation (J cm^{-2}) using a conversion factor of 4.56 μmol J^{-1}. We fitted the model resulting in estimates of GPP, ER, and NEP for each

day. Here, we multiplied the generated volumetric unit by mixing layer depth to report the estimates in area units (mmol O_2 m^{-2} d^{-1}) for ease of comparison with the results from mass-balance modeling. NEP values were converted to units of CO_2 assuming a quotient of 1 (mol C/mol O). We then matched the NEP data with NMP from mass-balance model based on the measured data.

Statistical analysis

We applied piecewise structural equation modeling (SEM) to interpret the causal and directional links between physical and biological parameters operating on CO_2 emissions. We constructed a network to simultaneously evaluate the climatic drivers and different pathways affecting reservoir CO_2. The network consists of two dependent layers of factor interaction: the first one is whether CO_2 emissions arise from environmental variables; the second one is whether the parallel variations of net metabolic CO_2 production and carbonate buffering determined the CO_2 emissions. To estimate the predictive strengths in both reservoirs, we fitted models for both reservoirs using the function *psem* in the R package *piecewiseSEM* (Lefcheck, 2016). The estimates of standardized path coefficients were reported for evaluating the effect sizes of each relationship (or path). The evaluation of goodness of fit and associated uncertainty was performed through the coefficient of determination (R^2) and the residual standard error (RSE), respectively. The overall fit of the model was evaluated using Shipley's test of d-separation: Fisher's C statistic (if $p > 0.05$, then no paths are missing and the model is a good fit). All modeling calculation and statistical analyses were performed in R version 3.5.1 (R Core Team, 2021).

Results

Physical and chemical characteristics of reservoirs

Overall, both reservoirs had similar seasonality, with Hassel having higher water residence time (WRT), alkalinity, DIC, DOC, and TP (**Fig. 2**, Wilcoxon test, $p \leq 0.001$). WRT in both reservoirs was driven by changes in discharge of inflows since the volumes of both reservoirs remained constant. During summer when both reservoirs were thermally stratified, decreases in inflow discharge were followed by increases in WRT (**Fig. 2**a and **Fig. S2**a). ΔO_2 ranged from -200 to 180 µmol L^{-1} with a median of -40 µmol L^{-1} in both reservoirs. Reservoirs were mostly undersaturated in O_2 with the exception of summer (**Fig. 2**b). Both reservoirs were characterized by longer residence time and higher nutrients in summer (**Fig. 2**a, c, d). The seasonality of alkalinity and TP (lower in early spring and higher in autumn) followed the opposite pattern as nitrate. pH values shared similar seasonal variations with alkalinity, ranging between 6.5 and 9.8 with 7.5

as the median. NO_3, alkalinity, and DIC in both reservoirs exhibit similar seasonal patterns to inflows (**Fig. S2**).

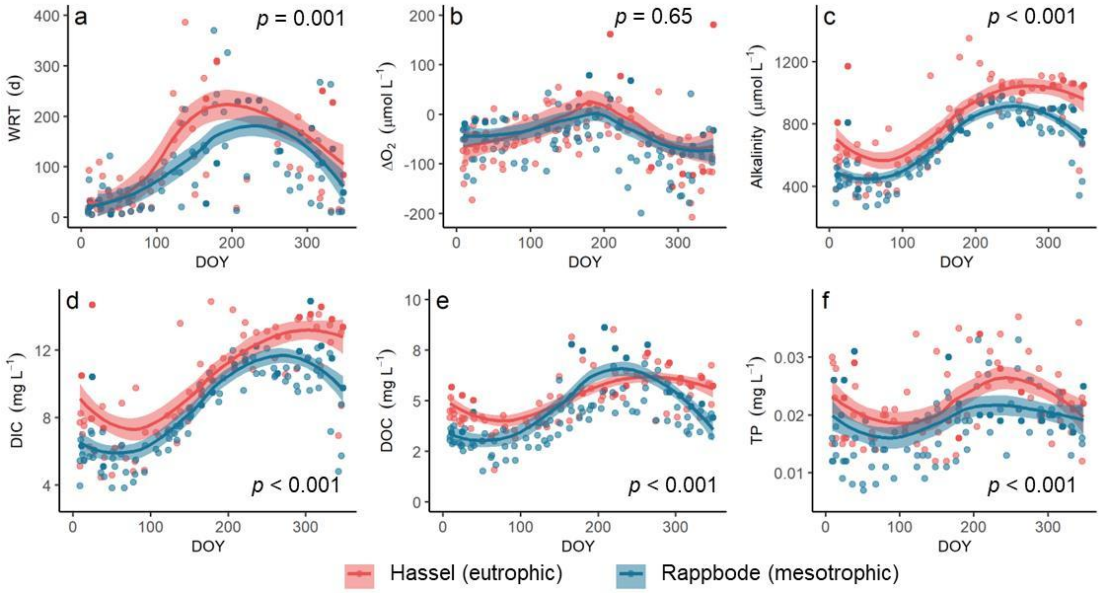

Figure 2. Seasonal variations in water residence time (WRT, a), O_2 departure from atmospheric equilibrium (ΔO_2, b), alkalinity (c), dissolved inorganic carbon (DIC, d), dissolved organic carbon (DOC, e), and total phosphorous (TP, f) in Hassel and Rappbode Reservoirs, respectively. Dots are the point measurements during the 8-year monitoring. Solid lines with shaded area in the time series plots are locally weight regression model fittings (loess) for visual interpretation of the temporal dynamics. The shaded area represents 95% confidence intervals. *p* values represent the significance of differences between both reservoirs by Wilcox tests. DOY: day of the year.

Both reservoirs were mainly supersaturated with CO_2 (**Fig. S3**). CO_2 was oversaturated in 232 out of 264 observations, with a median of 44 μmol L^{-1}. Additionally, ΔO_2 and ΔCO_2 for both reservoirs significantly negatively correlated with each other ($p \leq 0.001$). Both reservoirs showed an offset relative to the expected -1:1 line with larger offset in Hassel (200 and 90 μmol L^{-1} in Hassel and Rappbode according to the method from Vachon et al. (2020)). The slope of the linear regressions between ΔO_2 and ΔCO_2 for both reservoirs were lower than -1 (estimate = -1.21, R^2 = 0.27, $p < 0.001$).

Patterns of CO_2 emissions

On average, both reservoirs were net sources of CO_2 to the atmosphere, despite a few periods of CO_2 uptake in summer (**Fig. 3**). Inflows showed a clear difference in magnitude and seasonal variation of CO_2 concentrations compared to reservoirs (**Fig. 3**). Median CO_2 concentrations of the Hassel and Rappbode reservoirs were 22 and 23 μmol L^{-1}, respectively, which were much lower than 74 and 50 μmol L^{-1} in both inflows. CO_2 emission rates of reservoirs ranged from −28 to 348 mmol m^{-2} d^{-1}, with median values of 28 and 35 mmol m^{-2} d^{-1} in Hassel and Rappbode, respectively. Apart from the apparent seasonal variations, we did not find significant monotonic long-term trends in CO_2 emissions (Mann-Kendall test, $p > 0.05$). Given the ice-free period from April to December, annual mean CO_2 emissions from Hassel and Rappbode Reservoirs were estimated at 16.2 and 16.5 Mg C yr^{-1}, respectively. Both concentrations and emissions in reservoirs were higher in winter and lower in summer. Contrasting to significant difference of CO_2 concentrations between both inflows, CO_2 concentrations (t-test, $p = 0.27$) and emissions (t-test, $p = 0.56$) in the two reservoirs with divergent trophic states were not significantly different from each other.

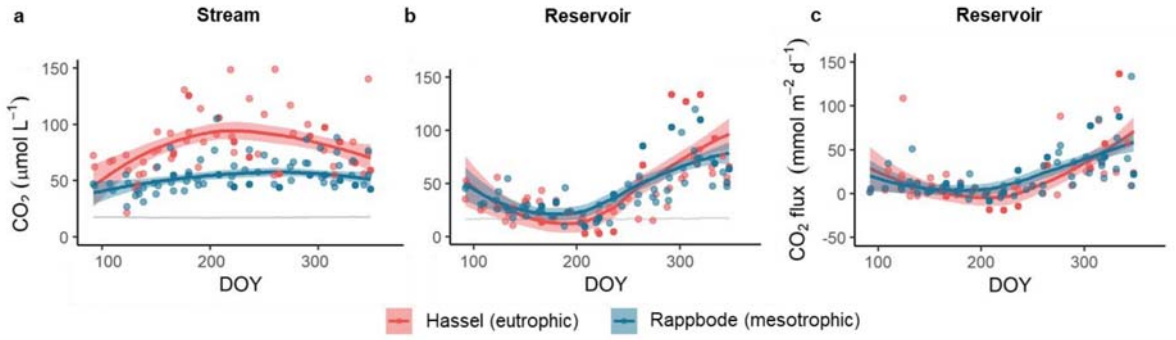

Figure 3. Seasonal variations in the CO_2 concentrations in the Hassel and Rappbode inlets (a) and Reservoirs (b) and fluxes in both reservoirs (c) and from April to December (full ice-covered period is excluded). Dots are the point measurements during the 8-year monitoring. The grey lines represent the atmospheric equilibrium concentration of CO_2. DOY: day of the year.

Given k_{CO2} and CO_2 concentration directly drive CO_2 emissions, we observed higher dependency between emissions and concentrations than between emissions and k_{CO2} in Hassel (the inclusion of k_{CO2} enhances the predictive power of linear regression model from 70% to 92%), whereas similar contribution of CO_2 concentrations and k_{CO2} to the variance of CO_2 emissions were observed in Rappbode (the predictive power of linear regression model increases from 41% to 91%). Regarding the relationships between CO_2 emissions and other environmental indices (**Fig. S4**), light (sunlight duration of the day, $p < 0.001$, $R^2 = 0.21$, n = 262) and pH ($p < 0.001$, $R^2 = 0.25$, n = 262) have stronger negative relationships with CO_2 emissions than did water temperature ($p < 0.001$, $R^2 = 0.15$, n = 262) and WRT ($p < 0.001$, $R^2 = 0.14$, n = 256). Compared to above

correlations, the positive link between nitrate and CO_2 emissions was rather moderate ($p < 0.001$, $R^2 = 0.05$, n = 262).

Mass balance modeling of CO_2 budgets

Mass balances of DIC and CO_2 were explored to provide evidence for the contributions of different processes supporting CO_2 evasion in reservoirs. Contributions of inflows to the CO_2 fluxes (mmol m^{-2} d^{-1}) in mass balance budget were close to 0 for the whole period (1^{st}-3^{rd} quartile: 1.3-6.0 mmol m^{-2} d^{-1}, **Fig. 4**a, b). That means that equal amounts of CO_2 entering the reservoir at the inflow also left the reservoir at the outflow.

Compared to the contribution of inflow (**Fig. S5**, median: 5.9% in Hassel and 4.2% in Rappbode), NMP and carbonate buffering were the primary contributors to net CO_2 emissions in both reservoirs (**Fig. S5**, median: 46% and 45% in Hassel; 57% and 39% in Rappbode). NMP varied remarkably following similar temporal patterns in both reservoirs, which decreased below 0 in summer (GPP>ER) and became positive again from autumn onwards. However, the variation range of NMP in Hassel was lower than in Rappbode (**Fig. 4**c, d). The variation in NMP (1^{st}-3^{rd} quartile: -19.0-42.0 mmol m^{-2} d^{-1}) in both reservoirs was larger than the one in CO_2 emissions (1^{st}-3^{rd} quartile: 5.6-30.0 mmol m^{-2} d^{-1}).

Carbonate buffering had opposite fluctuations compared to NMP with narrower variation ranges (1^{st}-3^{rd} quartile: -1.5-27.8 mmol m^{-2} d^{-1}, **Fig. 4**c, d), especially in the Rappbode Reservoir. As a result, despite NMP showed the possibility of CO_2 deficit in the systems, CO_2 mostly sustained outgassing during summer (CO_2 emissions > 0, **Fig. 4**e, f) due to the contribution of carbonate buffering. Due to lower alkalinity in Rappbode, CO_2 emissions were moderately modulated by carbonate buffering. Consequently, different variations of NMP and carbonate buffering between both reservoirs shaped similar temporal patterns of CO_2 emissions.

A negative correlation between the influence of NMP and carbonate buffering was observed with similar slopes (**Fig. 5**a, CB ~ NMP, Hassel: slope = -0.80, $p < 0.001$, $R^2 = 0.82$; Rappbode: slope = -0.89, $p < 0.001$, $R^2 = 0.89$). Regarding the median contributions of different sources over years, NMP and carbonate buffering were equally important to CO_2 dynamics in Hassel Reservoir, whereas there was a stronger influence of NMP on CO_2 dynamics in Rappbode Reservoir. All in all, CO_2 emissions were majorly driven by in-reservoir metabolic production and DIC import from the catchment.

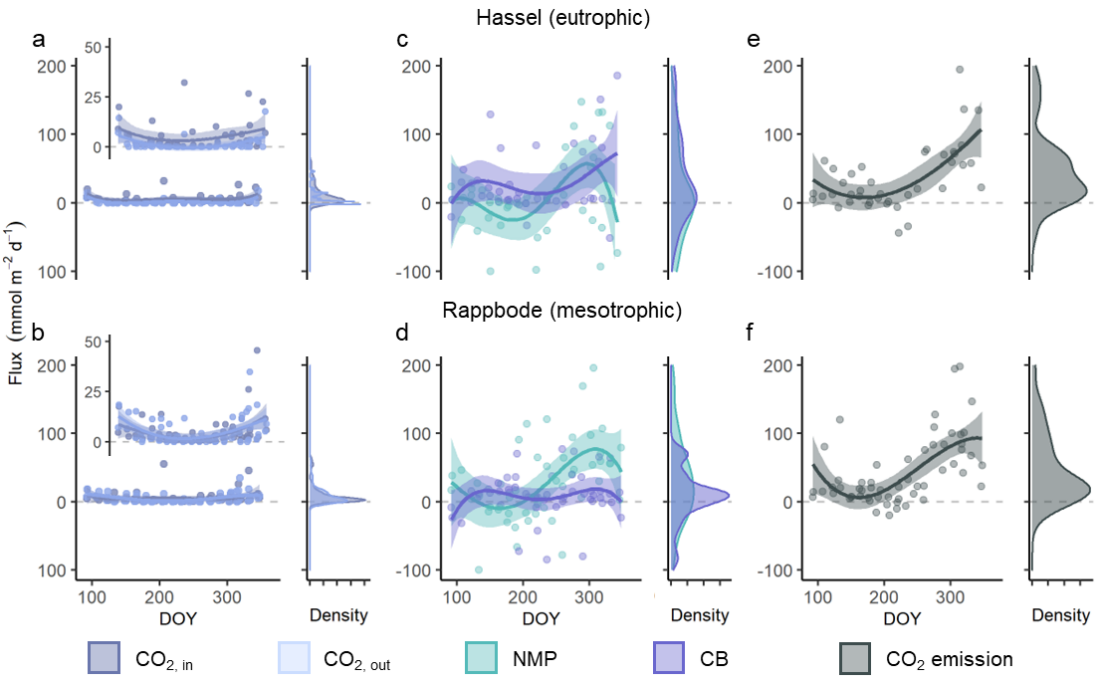

Figure 4. Season variations and density distributions of inlet input and outlet export flux of CO_2 (a and b), net metabolic CO_2 production (NMP) and carbonate buffering (CB, c and d), and CO_2 emissions (e and f) in areal CO_2 flux rates (mmol m^{-2} d^{-1}) from the results of coupling DIC-CO_2 mass-balance modeling in both reservoirs. Solid lines with shaded area in the time series plots are locally weight regression model fittings (loess) for visual interpretation of the temporal dynamics. The shaded area represents 95% confidence intervals. Fluxes of inputs and exports were normalized by dividing them by the surface area of the reservoir for comparison with other processes. The inner panels in a and b show the same seasonal variations in inflow input and outflow export in both reservoirs with a smaller scale. DOY: day of the year.

If the mixed layer depth increases, DIC rich hypolimnetic water is mixed into the epilimnion, increasing the epilimnetic DIC pool. This has an impact on NMP in our mass balance. We evaluated the potential influence of vertical DIC transfer on NMP in our model by multiplying DIC concentration by the volume of the water layer exchanged between epilimnion and hypolimnion (**Table 1**, see Supporting information **Text S2** for more details). Compared with NMP, the gain or release of hypolimnetic DIC was rather low at both reservoirs over the seasonal cycle except during autumn mixing (consistently below 5% and 12% of CO_2 produced or consumed via NMP in Hassel and Rappbode reservoir during 80% of the time, respectively, **Fig. S6**). During autumn turnover, some DIC may have been transported from the hypolimnion to the epilimnion. During this period, vertical input can account for up to 24% of estimated NMP to the upper layer in both reservoirs (**Fig. S6**b, c). Direct import of CO_2 from the hypolimnion was also limited due to the neutral pH in both reservoirs (Dadi et al., 2023), which means

453 that the majority of DIC was bicarbonate rather than CO_2. As a result, we
454 conclude that neglecting vertical input during mixing surely induced uncertainties
455 to the modelled NMP rates. This means that NMP cannot be equaled with -NEP
456 because a small part of the epilimnetic DIC pool change was resulting from
457 reservoir turnover. This is, however, not affecting our quantification of carbonate
458 buffering.

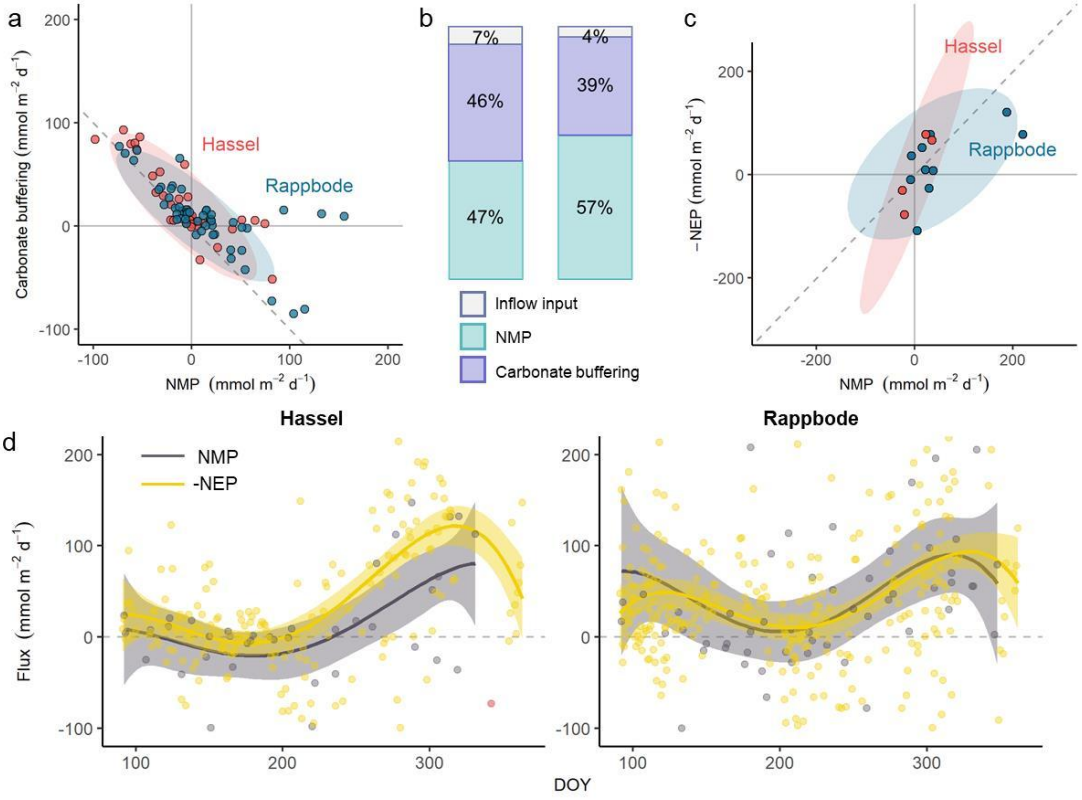

459

460 **Figure 5.** a. Correlations between carbonate buffering and net metabolic CO_2 production
461 (NMP) in Hassel (eutrophic) and Rappbode (mesotrophic) reservoirs during the ice-free
462 period. b. Median contributions of different processes to CO_2 emissions from the results of
463 coupling DIC-CO_2 mass-balance modeling in both reservoirs. c. Comparison between NMP
464 from mass-balance modeling and net ecosystem productivity (NEP) modeled from high-
465 frequency O_2 data. The dashed grey line is the 1:1 line, where the internal productivity
466 from both methods perfectly matches. d. Net metabolic CO_2 production expressed in areal
467 CO_2 rates estimated by mass balance calculations (grey dots) and whole-reservoir net
468 ecosystem metabolism (-NEP) derived from free-water oxygen measurements (yellow
469 dots). Seasonal smoothed trends are calculated using a fourth-degree polynomial
470 regression for net metabolic production (grey line) and -NEP (yellow line). The red dot as
471 the outlier in the Hassel Reservoir was excluded for generating the smoothed trend of NMP
472 to eliminate the effect on the smoothed line. Note here that positive values represent CO_2
473 production (net heterotrophy). DOY, day of the year.

To evaluate the reliability of the results from mass balance modeling, we estimated the -NEP by modeling the diel O_2 variation in the reservoir systems. The smoothed estimates of NMP from the mass balance model and -NEP from the lake metabolism model followed the same pattern across seasons (**Fig. 5**d). NMP and –NEP corresponded to the epilimnetic CO_2 concentrations during the stratified period. The offset between the two remained relatively conservative during summer.

Controls of CO_2 emissions

To infer the direct and indirect effects of light (sunlight duration), inflow discharge, DIC, and DOC with causal combination that underpin variations in CO_2 emissions we fitted a piecewise SEM model. The model explained 65% of the variation in CO_2 emissions from both reservoirs (**Fig. 6**). We found direct support for a negative relationship between light and NMP, and we did observe that lower inflow discharge was correlated with higher inflow DIC and in-reservoir DOC. CO_2 emissions were highest when NMP, carbonate buffering, and inflow CO_2 load were high. Variation in CO_2 emissions was primarily related to the patterns of NMP and carbonate buffering. While NMP also had negative effects on carbonate buffering, indicating both processes constrained each other.

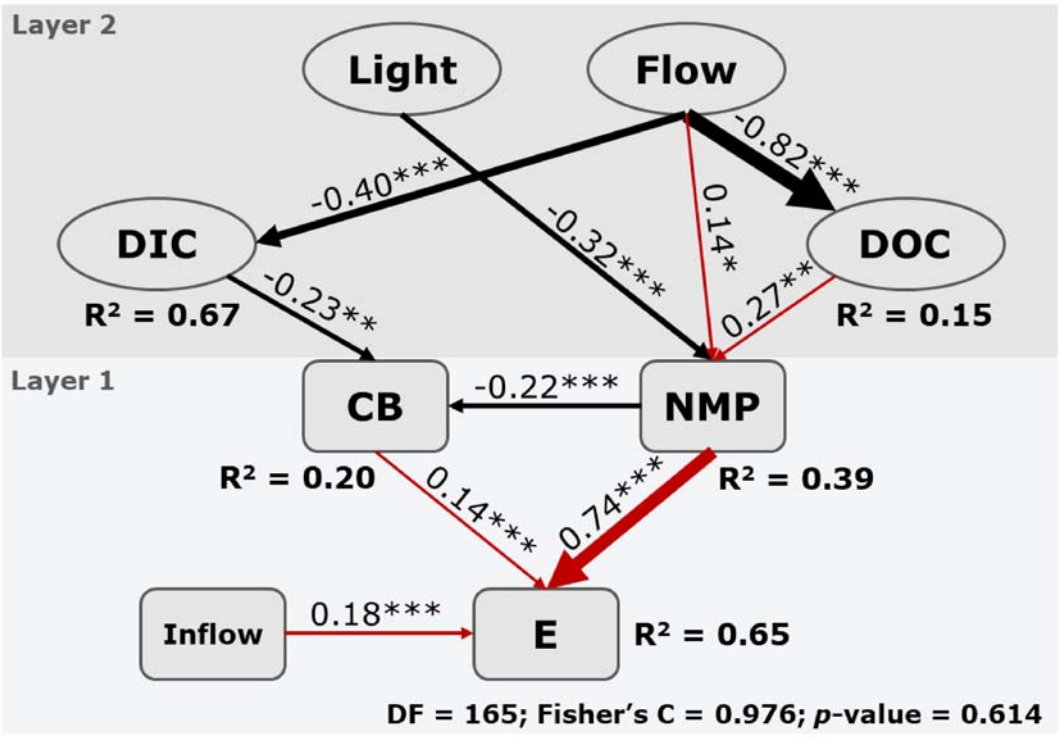

Figure 6. Structural equation model (SEM) representing connections between reservoir physical and biological parameters contributing to seasonal variations in CO_2 emissions (E). The SEM consisted of two dependent levels of factor interactions. Layer 1 assessed the influence of net metabolic CO_2 production (NMP), carbonate buffering (CB), and inflow CO_2

load on CO_2 emissions from reservoirs. Layer 2 assessed relationships between environmental variables (Light: sunlight duration of the day; Flow: inflow discharge; DIC: inflow DIC concentration; DOC: reservoir DOC concentration) and variations in CO_2 emissions. Note here that positive NMP represents CO_2 production (net heterotrophy). Black and red arrows represent statistically significant negative and positive effects, respectively ($p < 0.05$). Numbers adjacent to arrows are the standardized effect sizes of each relationship. *** $p < 0.001$; ** $p < 0.01$; * $p < 0.05$. Arrow width is proportional to the effect strength. SEM goodness of fit was evaluated based on variance explained by each of the two models (R^2). A summary of statistical outputs from the SEM model is provided in Supplementary Information **Table S2**.

Discussion

In this study, we observed that CO_2 emissions did not differ significantly between reservoirs with divergent trophic states. Instead, our results show that the carbonate system has a great potential to regulate the effect of net metabolic production on CO_2 emissions. This result extends observations by Marcé et al. (2015) that DIC inputs from catchments and the subsequent carbonate buffering need to be considered as an important contributor to CO_2 supersaturation to low alkalinity systems which can switch from CO_2 sources to weak CO_2 sinks. Primary productivity by itself is insufficient for estimations of CO_2 emissions from reservoirs. Ignoring the carbonate buffering capacity, therefore, is likely to result in a systematic bias towards underestimating CO_2 emissions. Our model approach offers quantitative insight on the potential contribution of carbonate buffering to the magnitude and seasonal variability of CO_2 in lakes and reservoirs under climate change.

Estimates of CO_2 emissions

The two reservoirs were CO_2 sources to the atmosphere over the annual cycle. The estimated CO_2 emissions from both reservoirs (62.3 and 67.9 g C m^{-2} yr^{-1}) confirm estimates from Halbedel and Koschorreck (2013) (74.9 and 87.6 g C m^{-2} yr^{-1}), which are based on much less data. Our estimates are similar to those of lake CO_2 emissions in temperate latitudes (Marcé et al., 2015), and to the overall magnitude and seasonal fluctuation of CO_2 emission from 39 German drinking reservoirs (Saidi and Koschorreck, 2017).

To assess the influence of sampling interval during estimates of annual CO_2 budgets in reservoirs, we randomly subsampled our biweekly dataset to simulate monthly, bimonthly, and seasonally sampling and compared the reconstructed total annual CO_2 fluxes to the original ones (**Fig. S7**). Artificially reducing our data density to monthly samplings resulted in virtually similar annual CO_2 emissions with the smallest variations (26% in Hassel and 20% in Rappbode).

Bimonthly sampling increased the error to 68% and 47% in both reservoirs, while seasonal-interval sampling will double the uncertainty. We therefore conclude that a bimonthly sampling frequency is probably an acceptable compromise between sampling effort and accuracy of the annual CO_2 budget.

We believe that omitting flood events would have little effect on our estimates of annual CO_2 emissions. We did not find substantial variations in CO_2 concentrations and emissions before, during, and after floods (**Fig. S8**), implying CO_2 chemostasis behavior (Aho et al., 2021). However, diffusive flux measurements should ideally be made frequently following ice out and then on a regular basis throughout the season until after mixing occurs in the fall (Wik et al., 2016).

We consider the uncertainty of *k* values has limited impact on the estimates of CO_2 emissions. CO_2 emissions were more regulated by CO_2 concentrations, rather than *k* (**Fig. S4**). Moreover, the range of wind speed at 1.5 m height typically varied within 2.0-3.3 m s^{-1} (1^{st}-3^{rd} quartile), resulting in a relatively narrow range of *k* variations (0.49-1.39 m d^{-1}).

Variations in surface area had little effect on CO_2 emission estimates or subsequent model results. Flood events rarely fluctuate the water levels due to surface-release dams (Wendt-Potthoff et al., 2014), and high banks prevent the occurrence of bank overflow at the conjunction parts between inflows and reservoirs (Leng et al., 2021). 90% of the water level data varied within 0.1m (**Fig. S9**), resulting in expansion or shrinkage in the surface area by 2.0% and 2.4% of the total surface area in Hassel and Rappbode, respectively.

Regarding spatial heterogeneity, both monitoring sites are representative of entire reservoirs as shown by direct CO_2 emission measurements using floating chambers along the reservoirs in 2015 (**Table S3**) (coefficient of variance among different sampling sites less than |0.35|), except the conjunction parts to the inflows which represent 17% and 12% of the total area of Hassel and Rappbode Reservoirs, respectively.

Contributions of processes to CO_2 emissions

CO_2 in reservoirs originates either from direct CO_2 inputs (inflows and groundwater), in-reservoir metabolism, or carbonate buffering (from ionic forms of carbonate to CO_2). The low contribution of inflow CO_2 in our study can be explained by the pH levels in both reservoirs, since DIC contributes primarily in the form of bicarbonate, instead of CO_2 as other studies (Wilkinson et al., 2016). Influence of CO_2 derived from the catchments was highest in spring probably due to high hydraulic loading and shorter residence time.

NMP explained most of the seasonal variations in CO_2 dynamics in both reservoirs (**Fig. 4** and **Fig. S5**e, f). The high-nutrient reservoir showed higher productivity during summer (more negative NMP), leading to an autotrophic system (Bogard and Del Giorgio, 2016; Halbedel and Koschorreck, 2013). Besides that, thermal stratification existed during this period (**Fig. S10**), which results in CO_2 depletion at the surface and CO_2 accumulation in the hypolimnion (Wendt-Potthoff et al., 2014). The accumulation of CO_2 in the hypolimnion is not important to NMP in the epilimnion, especially in eutrophic and deeper lakes (Brothers et al., 2012; Vachon et al., 2017), as exchange across the thermocline is limited (Kreling et al., 2014). When the water column becomes colder in autumn, however, NMP increased drastically in both reservoirs, coinciding with increased water column turnover and the associated mobilization of hypolimnetic CO_2 (Vachon and Del Giorgio, 2014). Increased external DOC loading during autumn could be another potential source supporting pelagic respiration during autumn (**Fig. 2**e), dominating the net metabolic production (Morling et al., 2017; Vachon et al., 2017). This is nicely confirmed by the positive connection between DOC and NMP from the SEM results (**Fig. 6**) and the simulated ecosystem metabolism results.

The comparison of NMP from the mass balance model with the estimated CO_2 production (–NEP) from LakeMetabolizer allows us to validate the reliability of our model. The coupling between the two approaches showed that the NMP mostly resulted from –NEP while other biotic processes had limited impact on NMP. The metabolism model yields slightly lower estimate than the mass balance model (**Fig. 5**c, slope = -0.77, R^2 = 0.43, p = 0.006). This can theoretically be attributed to additional biochemical and photochemical reactions included in NMP. However, photochemical CO_2-production was probably of minor importance since it only contributed 3% to total CO2 production in boreal lakes (Allesson et al., 2021). Anerobic processes in the epilimnion can be ruled out in our case given the fact that no changes of solutes were observed in water samples from both reservoirs incubated under in situ temperature and O_2 conditions (Dadi et al., 2023).

The uncertainty resulting from the chosen respiratory quotient to convert the unit of -NMP from mmol O_2 m^{-2} d^{-1} to mmol CO_2 m^{-2} d^{-1}, in our opinion, may be more essential in evaluating the comparability of NMP and -NEP (Berggren et al., 2012; Trentman et al., 2023). Compared to a reported respiratory quotient of 1.2 (Berggren et al., 2012), the quotient of 1:1 we used would underestimate the CO_2 production from metabolic processes. However, there was a large day-to-day variation in –NEP (**Fig. 5**d), reflecting the large variability in average daily CO_2 production in the epilimnion. Overall, the excellent agreement between mass balance and metabolism calculations underlines the reliability of our approach

under the studied time scale, whereas differences in chosen quotient and gas exchange between O_2 and CO_2 can generate a decoupling between both gases (Vachon et al., 2020).

Our mass balance model suggests a clear effect of the carbonate system on the size of the reservoir CO_2 pool. For both reservoirs, we found seasonal variations in CO_2 losses to and gains from carbonates. In addition, carbonate buffering can cause CO_2 production without O_2 consumption, uncoupling departure of O_2 and CO_2 (deviation from the 1:-1 line in **Fig. S3**). For both reservoirs, high positive carbonate buffering was observed in late spring and early summer along with the peak of external inorganic carbon contribution (**Fig. S5**c-f). This mechanism could be attributed to the ready replacement of evading and consumed CO_2 by external-derived carbonates. This leads to the coincidence of lowest net metabolic production and highest carbonate buffering (**Fig. 5**e, f), consequently attenuated seasonal variations in CO_2. Likewise, in autumn, when metabolic activity produces CO_2, the external carbonate source was able to shift carbonate equilibria from CO_2 towards carbonates, resulting in lower CO_2 emissions. During summer (~220-260 day of year), not only was stream discharge low, but also was the mixing layer depth (**Fig. S10**). This results in small absolute amounts of metabolic production and carbonate buffering but comparatively large importance of carbonate buffering (**Fig. S5**). Seasonal temperature increase can also lower the solubility of CO_2, eventually altering CO_2 gradient across the water-air interface. Apart from high alkalinity systems, which might cause seasonal variations in CO_2 emissions to be independent of NEP (Marcé et al., 2015), we emphasize that even in system with moderate alkalinity, the carbonate buffering capacity needs to be considered in seasonal CO_2 budgets, notably during summer, when it can contribute up to 50% of CO_2 emissions.

The estimated reservoir CO_2 budgets provide evidence how in-reservoir metabolic processes and carbonate buffering modulate the seasonal variations in CO_2 evasion in low-alkalinity systems. The mass balance model developed by Vachon et al. (2017) considered the shifting pH brought by CO_2 production and consumption, and hence DIC speciation equilibrium, to play a minimal impact. This is reasonable in lakes and reservoirs with low alkalinity/pH (Soued and Prairie, 2021; Vachon et al., 2017). In high pH reservoirs the mass-balance models took the extra carbonate precipitation into account (Finlay et al., 2010; López et al., 2011). Our study complements the findings from Marcé et al. (2015) that highlighted DIC generated from catchment weathering could potentially account for half of the emissions in temperate latitudes. McDonald et al. (2013) and Weyhenmeyer et al. (2015) documented the widespread DIC loading in determining lake CO_2, and pointed out the necessity to consider the temporal variability in hydrologic DIC inputs. Our findings reveal that the external DIC load

and carbonate buffering are not always coupled over time. Alternatively, once the reservoirs receive external inputs, the exchange between carbonates and CO_2 would only take place when there was a difference in alkalinity between the inflow and receiving water – that is especially in high pH situations.

Implications to current CO_2 budgets and future predictions

Reservoirs are currently confronted by a wide array of changes due to climate change, posing a threat to water resource security as well as changing C cycling. Altered rainfall pattern are affecting input of nutrients into reservoirs. Indirect effects of climate change, such as deforestation, as happening in the Rappbode catchment and resulting in 17% of forest loss in 2020 alone (Kong et al., 2022), lead to enhanced nutrient export from the catchment to reservoirs through surface runoff and leaching processes. Our SEM results indicate that from the seasonal perspective, drought not only raises in-reservoir DOC, leading to higher metabolic CO_2 production, but also increases external DIC import. Reservoir productivity is highest when light and drought coincide (summer) (Halbedel and Koschorreck, 2013). The general pattern of CO_2 regulation seems to be relatively independent of trophic state (**Fig. 3** and **Fig. S4**). Thus, classifying reservoirs according to catchment alkalinity might be more relevant for predicting CO_2 emissions than looking at trophic state.

We strongly recommend including carbonate buffering and its response to environmental change in future scenarios for predicting the effects of global change in lentic systems with low alkalinity. This is because the carbonate system is much more sensitive to the changes in in-reservoir processes than in high alkalinity systems, where carbonate buffering would behave more independent of NEP. Previous studies showed that alkalinity in more than 50% of global reservoirs and lakes is less than 1 meq L^{-1} (Marcé et al., 2015). Consideration of the offsetting effect of carbonate buffering will largely reduce the uncertainty of global inland water CO_2 emission estimations. In our reservoirs, we show that ruling out the link between CO_2 emissions and external DIC input would result in up to 72% of unexplainable CO_2 emissions. Concentrations of nutrients and inorganic carbon in inflows reach the peak for the year simultaneously (**Fig. S2**), thus the eutrophication (consumes CO_2 due to larger algal production) and allochthonous inorganic carbon input (shifts in carbonate equilibrium) impact CO_2 emissions concurrently in opposite directions (**Fig. 1**a).

Conclusions

Our process-based mass balance model approach based on the large data set collected over multiple years in two reservoirs suggests that not only the effects of elevated nutrient loads and eutrophication on CO_2 need to be considered.

Changed loads of DIC may exhibit an equally important effect on reservoir CO_2 emissions. Consistent with our hypothetical responses of reservoir CO_2 emissions (**Fig. 1**b), our study indicates that (1) each process influencing CO_2 budgets varies seasonally in an opposite direction, explaining a more conservative seasonal CO_2 dynamics, and (2) current models of reservoir CO_2 dynamics that are based solely on internal metabolism miss a substantial portion of CO_2 produced from external DIC inputs.

Our model approach should also be applicable in determining the carbon budgets in natural lakes beyond our study sites, because the principles regulating carbon cycling in different aquatic systems would be highly similar. Even though further research is still needed to incorporate the fate of terrestrial carbon and in-reservoir metabolic processing, we recommend particularly the inclusion of carbonate buffering into carbon budgets, to reduce uncertainty in predicting lake and reservoir CO_2 emissions under global change.

Acknowledgement

This study was financially supported by the Helmholtz Association within the project TERENO. Peifang Leng is supported by the CSC-DAAD Joint Fellowship Programme for postdocs and China Postdoctoral Science Foundation (No. 2022M723122). Thanks to Talsperrenbetrieb Sachsen-Anhalt (TSB) for providing hydrological data. We thank the UFZ Lake Research team for performing the monitoring. Special thanks to Karsten Rahn and Martin Wieprecht for field sampling and CO_2 analysis and to Burkhard Kühn for running the online probes. Thanks to Dr. Jörg Tittel, Dr. Katrin Wendt-Potthoff, Dr. Martin Schultze, and other colleagues at the Helmholtz Centre for Environmental Research (UFZ) for data supporting and helpful discussions. Thanks to Dr. Xiangzhen Kong for provision of the map and mixing layer depth. Thanks to Prof. Andreas Lorke, Dr. Clara Mendoza-Lera, Dr. Lorenzo Rovelli, and other colleges from University of Koblenz-Landau for providing valuable comments. We declare no conflict of interest. Datasets for this research can be found online at https://doi.org/10.6084/m9.figshare.21954008.v1.

References:

Aho, K.S., Fair, J.H., Hosen, J.D., Kyzivat, E.D., Logozzo, L.A., Rocher-Ros, G., Weber, L.C., Yoon, B. and Raymond, P.A. 2021. Distinct concentration-discharge dynamics in temperate streams and rivers: CO_2 exhibits chemostasis while CH_4. Limnology and Oceanography 66(10), 3656-3668.

Allesson, L., Koehler, B., Thrane, J.-E., Andersen, T. and Hessen, D.O. 2021. The role of photomineralization for CO_2 emissions in boreal lakes along a gradient of dissolved organic matter. Limnology and Oceanography 66(1), 158-170.

Barth, J.A.C., Mader, M., Nenning, F., van Geldern, R. and Friese, K. 2017. Stable isotope mass balances versus concentration differences of dissolved inorganic carbon – implications for tracing carbon turnover in reservoirs. Isotopes in Environmental and Health Studies 53(4), 413-426.

Berggren, M., Lapierre, J.-F. and del Giorgio, P.A. 2012. Magnitude and regulation of bacterioplankton respiratory quotient across freshwater environmental gradients. The ISME Journal 6(5), 984-993.

Bogard, M.J. and Del Giorgio, P.A. 2016. The role of metabolism in modulating CO_2 fluxes in boreal lakes. Global Biogeochemical Cycles 30(10), 1509-1525.

Brothers, S.M., Prairie, Y.T. and del Giorgio, P.A. 2012. Benthic and pelagic sources of carbon dioxide in boreal lakes and a young reservoir (Eastmain-1) in eastern Canada. 26(1).

Burchard, H. and Bolding, K. 2001. Comparative Analysis of Four Second-Moment Turbulence Closure Models for the Oceanic Mixed Layer. Journal of Physical Oceanography 31(8), 1943-1968.

Chaplot, V. and Mutema, M. 2021. Sources and main controls of dissolved organic and inorganic carbon in river basins: A worldwide meta-analysis. Journal of Hydrology 603, 126941.

Crusius, J. and Wanninkhof, R. 2003. Gas transfer velocities measured at low wind speed over a lake. Limnology & Oceanography 48(3), 1010-1017.

Dadi, T., Friese, K., Wendt-Potthoff, K., Marcé, R. and Koschorreck, M. 2023. Oxygen Dependent Temperature Regulation of Benthic Fluxes in Reservoirs. Global Biogeochemical Cycles 37(4).

Deemer, B.R., Harrison, J.A., Li, S., Beaulieu, J.J., DelSontro, T., Barros, N., Bezerra-Neto, J.F., Powers, S.M., dos Santos, M.A. and Vonk, J.A. 2016. Greenhouse Gas Emissions from Reservoir Water Surfaces: A New Global Synthesis. BioScience 66(11), 949-964.

DelSontro, T., Beaulieu, J.J. and Downing, J.A. 2018. Greenhouse gas emissions from lakes and impoundments: Upscaling in the face of global change. Limnology & Oceanography: Letters 3(3), 64-75.

Duvert, C., Bossa, M., Tyler, K.J., Wynn, J.G., Munksgaard, N.C., Bird, M.I., Setterfield, S.A. and Hutley, L.B. 2019. Groundwater-Derived DIC and Carbonate Buffering Enhance Fluvial CO_2 Evasion in Two Australian Tropical Rivers. Journal of Geophysical Research: Biogeosciences 124(2), 312-327.

Finlay, K., Leavitt, P.R., Patoine, A., Patoine, A. and Wissel, B. 2010. Magnitudes and controls of organic and inorganic carbon flux through a chain of hard-water lakes on the northern Great Plains. Limnology and Oceanography 55(4), 1551-1564.

Friese, K., Schultze, M., Boehrer, B., Büttner, O., Herzsprung, P., Koschorreck, M., Kuehn, B., Rönicke, H., Tittel, J., Wendt-Potthoff, K., Wollschläger, U., Dietze, M. and Rinke, K. 2014.

763 Ecological response of two hydro-morphological similar pre-dams to contrasting land-use in
764 the Rappbode reservoir system (Germany). International Review of Hydrobiology 99(5), 335-
765 349.
766 Gattuso, J.-P., Epitalon, J.-M., H., L. and J., O. 2021 seacarb: seawater carbonate chemistry, R
767 package version 3.3.0. http://CRAN.R-project.org/package=seacarb.
768 Halbedel, S. and Koschorreck, M. 2013. Regulation of CO_2 emissions from temperate streams and
769 reservoirs. Biogeosciences 10(11), 7539-7551.
770 Holtgrieve, G.W., Schindler, D.E., Branch, T.A. and A'Mar, Z.T. 2010. Simultaneous quantification of
771 aquatic ecosystem metabolism and reaeration using a Bayesian statistical model of oxygen
772 dynamics. Limnology and Oceanography 55(3), 1047-1063.
773 Hope, D., Palmer, S.M., Billett, M.F. and Dawson, J.J.C. 2001. Carbon dioxide and methane evasion
774 from a temperate peatland stream. Limnology and Oceanography 46(4), 847-857.
775 IPCC, W.G.I. 2022 Climate change 2022: Impacts, adaptation and vulnerability. Pörtner, H.-O.,
776 Roberts, D.C., Adams, H., Adler, C., Aldunce, P., Ali, E., Begum, R.A., Betts, R., Kerr, R.B.
777 and Biesbroek, R. (eds).
778 Jones, J.R., Obrecht, D.V., Graham, J.L., Balmer, M.B., Filstrup, C.T. and Downing, J.A. 2016.
779 Seasonal patterns in carbon dioxide in 15 mid-continent (USA) reservoirs. Inland Waters
780 6(2), 265-272.
781 Khan, H., Laas, A., Marcé, R. and Obrador, B. 2020. Major Effects of Alkalinity on the Relationship
782 Between Metabolism and Dissolved Inorganic Carbon Dynamics in Lakes. Ecosystems 23(8),
783 1566-1580.
784 Kong, X., Ghaffar, S., Determann, M., Friese, K., Jomaa, S., Mi, C., Shatwell, T., Rinke, K. and Rode,
785 M. 2022. Reservoir water quality deterioration due to deforestation emphasizes the
786 indirect effects of global change. Water Research 221, 118721.
787 Kortelainen, P., Rantakari, M., Huttunen, J.T., Mattsson, T., Alm, J., Juutinen, S., Larmola, T., Silvola,
788 J. and Martikainen, P.J. 2006. Sediment respiration and lake trophic state are important
789 predictors of large CO_2 evasion from small boreal lakes. Glob Chang Biol 12(8), 1554-1567.
790 Koschorreck, M., Prairie, Y.T., Kim, J. and Marcé, R. 2021. Technical note: CO_2 is not like CH_4 –
791 limits of and corrections to the headspace method to analyse pCO_2 in fresh water.
792 Biogeosciences 18(5), 1619-1627.
793 Kreling, J., Bravidor, J., McGinnis, D.F., Koschorreck, M. and Lorke, A. 2014. Physical controls of
794 oxygen fluxes at pelagic and benthic oxyclines in a lake. Limnology and Oceanography 59(5),
795 1637-1650.
796 Lapierre, J.-F., Guillemette, F., Berggren, M. and del Giorgio, P.A. 2013. Increases in terrestrially
797 derived carbon stimulate organic carbon processing and CO_2 emissions in boreal aquatic
798 ecosystems. Nature Communications 4(1), 2972.
799 Lefcheck, J.S. 2016. piecewiseSEM: Piecewise structural equation modelling in r for ecology,
800 evolution, and systematics. Methods in Ecology and Evolution 7(5), 573-579.
801 Leng, P., Kamjunke, N., Li, F. and Koschorreck, M. 2021. Temporal Patterns of Methane Emissions
802 From Two Streams With Different Riparian Connectivity. Journal of Geophysical Research:
803 Biogeosciences 126(8).
804 Li, Y., Shang, J., Zhang, C., Zhang, W., Niu, L., Wang, L. and Zhang, H. 2021. The role of
805 freshwater eutrophication in greenhouse gas emissions: A review. Science of The Total
806 Environment 768, 144582.

López, P., Marcé, R. and Armengol, J. 2011. Net heterotrophy and CO_2 evasion from a productive calcareous reservoir: Adding complexity to the metabolism-CO_2 evasion issue. Journal of Geophysical Research: Biogeosciences 116(G2).

Marcé, R., Obrador, B., Morguí, J.-A., Lluís Riera, J., López, P. and Armengol, J. 2015. Carbonate weathering as a driver of CO_2 supersaturation in lakes. Nature Geoscience 8(2), 107-111.

McDonald, C.P., Stets, E.G., Striegl, R.G. and Butman, D. 2013. Inorganic carbon loading as a primary driver of dissolved carbon dioxide concentrations in the lakes and reservoirs of the contiguous United States. Global Biogeochemical Cycles 27(2), 285-295.

Morling, K., Herzsprung, P. and Kamjunke, N. 2017. Discharge determines production of, decomposition of and quality changes in dissolved organic carbon in pre-dams of drinking water reservoirs. Science of The Total Environment 577, 329-339.

Parkhurst, D.L. and Appelo, C.A.J. 2013 Description of input and examples for PHREEQC version 3: a computer program for speciation, batch-reaction, one-dimensional transport, and inverse geochemical calculations, p. 519, Reston, VA.

Pi, X., Luo, Q., Feng, L., Xu, Y., Tang, J., Liang, X., Ma, E., Cheng, R., Fensholt, R., Brandt, M., Cai, X., Gibson, L., Liu, J., Zheng, C., Li, W. and Bryan, B.A. 2022. Mapping global lake dynamics reveals the emerging roles of small lakes. Nature Communications 13(1), 5777.

R Core Team 2021 A language and environment for statistical computing. R Foundation for Statistical Computing, Vienna, Austria.

Saidi, H. and Koschorreck, M. 2017. CO_2 emissions from German drinking water reservoirs. Science of The Total Environment 581-582, 10-18.

Soued, C. and Prairie, Y.T. 2021. Changing sources and processes sustaining surface CO_2 and CH_4 fluxes along a tropical river to reservoir system. Biogeosciences 18(4), 1333-1350.

Stets, E.G., Butman, D., McDonald, C.P., Stackpoole, S.M., DeGrandpre, M.D. and Striegl, R.G. 2017. Carbonate buffering and metabolic controls on carbon dioxide in rivers. Global Biogeochemical Cycles 31(4), 663-677.

Stets, E.G., Striegl, R.G., Aiken, G.R., Rosenberry, D.O. and Winter, T.C. 2009. Hydrologic support of carbon dioxide flux revealed by whole-lake carbon budgets. Journal of Geophysical Research 114(G1).

Tittel, J., Hüls, M. and Koschorreck, M. 2019. Terrestrial Vegetation Drives Methane Production in the Sediments of two German Reservoirs. Scientific Reports 9(1), 15944.

Tittel, J., Müller, C., Schultze, M., Musolff, A. and Knöller, K.J.B. 2015. Fluvial radiocarbon and its temporal variability during contrasting hydrological conditions. Biogeochemistry 126(1), 57-69.

Trentman, M.T., Hall, R.O. and Valett, H.M. 2023. Exploring the mismatch between the theory and application of photosynthetic quotients in aquatic ecosystems. Limnology and Oceanography Letters.

Trolle, D., Staehr, P.A., Davidson, T.A., Bjerring, R., Lauridsen, T.L., Søndergaard, M. and Jeppesen, E. 2012. Seasonal Dynamics of CO_2 Flux Across the Surface of Shallow Temperate Lakes. Ecosystems 15(2), 336-347.

Umlauf, L. and Lemmin, U. 2005. Interbasin exchange and mixing in the hypolimnion of a large lake: The role of long internal waves. Limnology and Oceanography 50(5), 1601-1611.

Vachon, D. and Del Giorgio, P.A. 2014. Whole-Lake CO_2 Dynamics in Response to Storm Events in Two Morphologically Different Lakes. Ecosystems 17(8), 1338-1353.

Vachon, D., Sadro, S., Bogard, M.J., Lapierre, J.F., Baulch, H.M., Rusak, J.A., Denfeld, B.A., Laas, A., Klaus, M., Karlsson, J., Weyhenmeyer, G.A. and Giorgio, P.A. 2020. Paired O_2 – CO_2 measurements provide emergent insights into aquatic ecosystem function. Limnology and Oceanography Letters 5(4), 287-294.

Vachon, D., Solomon, C.T. and Del Giorgio, P.A. 2017. Reconstructing the seasonal dynamics and relative contribution of the major processes sustaining CO_2 emissions in northern lakes. Limnology and Oceanography 62(2), 706-722.

Wendt-Potthoff, K., Kloß, C., Schultze, M. and Koschorreck, M. 2014. Anaerobic metabolism of two hydro-morphological similar pre-dams under contrasting nutrient loading (Rappbode Reservoir System, Germany). International Review of Hydrobiology 99(5), 350-362.

Weyhenmeyer, G.A., Kosten, S., Wallin, M.B., Tranvik, L.J., Jeppesen, E. and Roland, F. 2015. Significant fraction of CO_2 emissions from boreal lakes derived from hydrologic inorganic carbon inputs. Nature Geoscience 8(12), 933-936.

Wik, M., Thornton, B.F., Bastviken, D., Uhlbäck, J. and Crill, P.M. 2016. Biased sampling of methane release from northern lakes: A problem for extrapolation. Geophysical Research Letters 43(3).

Wilkinson, G.M., Buelo, C.D., Cole, J.J. and Pace, M.L. 2016. Exogenously produced CO_2 doubles the CO_2 efflux from three north temperate lakes. Geophysical Research Letters 43(5), 1996-2003.

Winslow, L., Read, J., Woolway, R., Brentrup, J., Leach, T., Zwart, J., Albers, S. and Collinge, D. 2019. Package 'rLakeAnalyzer'. Lake Physics Tools.

Winslow, L.A., Zwart, J.A., Batt, R.D., Dugan, H.A., Woolway, R.I., Corman, J.R., Hanson, P.C. and Read, J.S. 2016. LakeMetabolizer: an R package for estimating lake metabolism from free-water oxygen using diverse statistical models. Inland Waters 6(4), 622-636.

Wouters, R.J.W.u.A. 2011. The Bodewerk; Das Bodewerk. 13.

Xiao, Q., Xu, X., Duan, H., Qi, T., Qin, B., Lee, X., Hu, Z., Wang, W., Xiao, W. and Zhang, M. 2020. Eutrophic Lake Taihu as a significant CO_2 source during 2000–2015. Water Research 170, 115331.